

Article

Field Test on Buoyancy Variation of a Subsea Bottom-Supported Foundation Model

Tianyi Fang ¹, Guojun Liu ², Guanlin Ye ^{1,*}, Shang Pan ¹, Haibin Shi ² and Lulu Zhang ¹

¹ State Key Laboratory of Ocean Engineering, Department of Civil Engineering, Shanghai Jiao Tong University, Shanghai 200240, China; fty1994@sjtu.edu.cn (T.F.); freedom0623@sjtu.edu.cn (S.P.); lulu_zhang@sjtu.edu.cn (L.Z.)

² Shanghai Zhenhua Heavy Industries Co., Ltd (ZPMC), Shanghai 200125, China; liuguojun@zpmc.com (G.L.); shihaibin@zpmc.com (H.S.)

* Correspondence: ygl@sjtu.edu.cn; Tel.: +86-2-134-204-833

Received: 29 March 2019; Accepted: 10 May 2019; Published: 13 May 2019



Abstract: The bottom-supported foundation is the most important component of offshore platforms, as it provides the major support to the upper structure. The buoyancy of the bottom-supported foundation is a critical issue in platform design because it counteracts parts of the vertical loads. In this paper, a model box was designed and installed with earth pressure transducers and pore pressure transducers to simulate the sitting process of the bottom-supported foundation. The buoyancy acting on the model box was calculated on the basis of two different methods, i.e., the water pressure difference between top and bottom surface and the effective stress at the bottom of the model. Field tests with different sitting times were carried out on the saturated soft clay seabed. Numerical coupled analysis was performed to verify the dissipation of the excess pore pressure at the bottom of the model. The results showed that the buoyancy of the model could reach twice the calculated value of Archimedes' law in the initial stage, however, it eventually stabilized near the theoretical value as the excess pore pressure dissipated. There was a slight fluctuation in buoyancy due to the phase lag of the pore pressure response caused by the low permeability of the seabed.

Keywords: buoyancy; pore pressure; bottom-supported foundation; field test; numerical analysis

1. Introduction

The offshore platform has good applicability in shallow sea areas with flat clayey seabed because of its relatively low requirement of soil-bearing capacity. Generally, such platform can be divided into an upper structure and a bottom-supported foundation. The latter is usually designed to be hollow, with a larger bottom area to provide sufficient support. The buoyancy of the bottom-supported foundation is an important part of the support force, since it counteracts parts of the vertical loads. Therefore, it is very important for the design of offshore platforms to investigate the buoyancy variation of the bottom-supported foundation during the whole operation process.

The existing researches regarding the buoyancy of structures are basically focused on underground structures embedded in saturated soils. The buoyancy acting on the structure varies depending on the type of the soil (clay or sand). It is proved that the buoyancy of a structure in saturated sand is almost equal to the calculated value of Archimedes' law [1,2]. When liquefaction occurs, the buoyancy is much greater than that in hydrostatic state [3–5]. The problem of buoyancy in weakly permeable soils like clay is usually investigated with indoor model test. The bucket model is usually used to simulate the underground structure, and the additional weight is adjusted to control whether the bucket is floating or not. The results of these researches show that the measured buoyancy is less than the theoretical value based on Archimedes' law, especially in clays [6,7]. The phenomenon of reduced

buoyancy is explained by some microscopic-level studies [8,9]. Furthermore, the buoyancy acting on the underground structure is also affected by the hydraulic gradient depending on the soil type. Indoor model tests and numerical analysis were carried out to study the effect of seepage on buoyancy. The results show that the buoyancy of a structure is greater than the theoretical value, considering the vertical seepage [10]. In the aforementioned studies, the buoyancy measurements were carried out only after the structure was embedded in the soil. For offshore platforms, attention should be paid to the point of the contact between the bottom-supported foundation and the seabed.

In this paper, field tests based on the characteristics of the bottom-supported foundation were carried out. A model box was designed with earth pressure and pore pressure transducers to simulate the entire operation process of such foundation. The buoyancy acting on the model box can be calculated on the basis of two different methods, i.e., the water pressure difference between top and bottom surface and the effective stress at the bottom of the model. Five tests were performed, with a sitting time of 3 h, 6 h, 22 h, 2.5 days, and 5 days, and the sitting time was calculated from the time the model contacted the seabed. The buoyancy variation was recorded during the entire sitting time. The effect of tides on buoyancy was also considered during the tests. The test revealed the variation of buoyancy acting on the model and the excess pore pressure dissipation at the bottom of the model. A coupled finite-element analysis was performed to verify the dissipation of the excess pore pressure using the Modified Cam Clay (MCC) model [11,12], and the comparison of buoyancy was made between the simulation and the measured values.

2. Field Tests

The site of this field test is located in the East China Sea, as shown in Figure 1. It is characterized by a soft clay seabed, with water depth of about 5 m and tidal difference of about 2.5 m. The test was executed in the industrial area of Changxing Island.

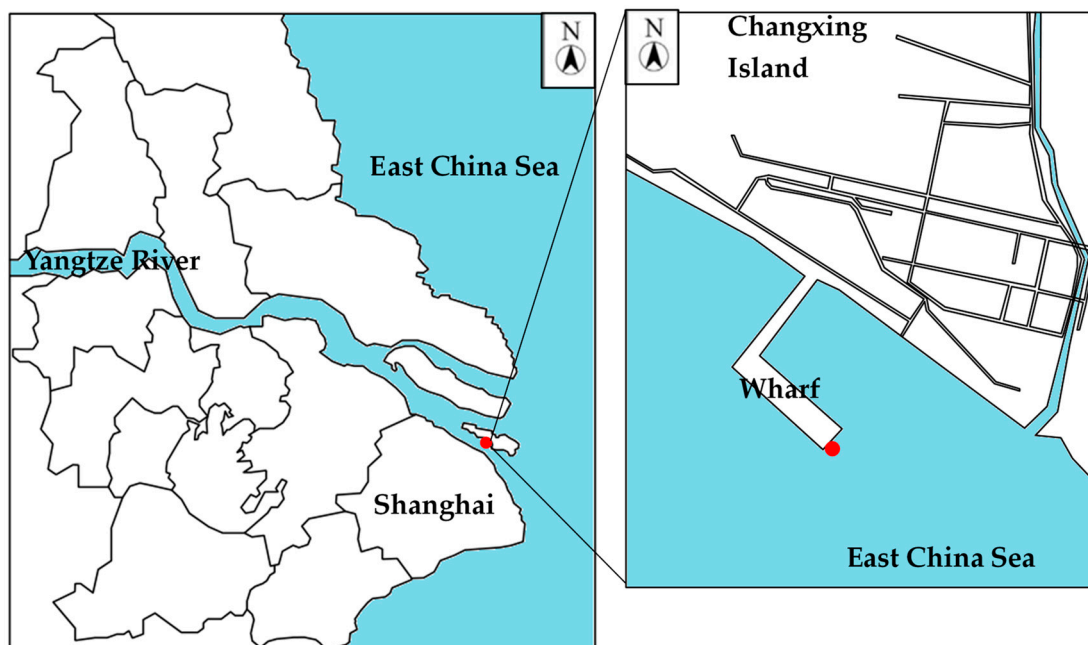


Figure 1. Schematic diagram of the test site.

2.1. Test Model

In the field test, a hollow cuboid sealing box model was used to simulate the bottom-supported foundation. The size of the model box was $2\text{ m} \times 2\text{ m} \times 1\text{ m}$, and the weight was 10 tons, which can be considered to be proportional to the real field condition. It was connected to a crane by a dynamometer,

whose real-time readings were recorded using a computer. A total of seven pore pressure transducers were used to measure the pore water pressure, one on the top and six at the bottom of the model. Five earth pressure transducers were installed at the bottom of the model to measure the total stress. The readings of all the transducers were recorded in the data acquisition instrument at a defined time interval. The theoretical buoyancy of the model was 40 kN when it was completely submerged in water. Figure 2 shows the overall and bottom schematic diagram of the aforementioned box model.

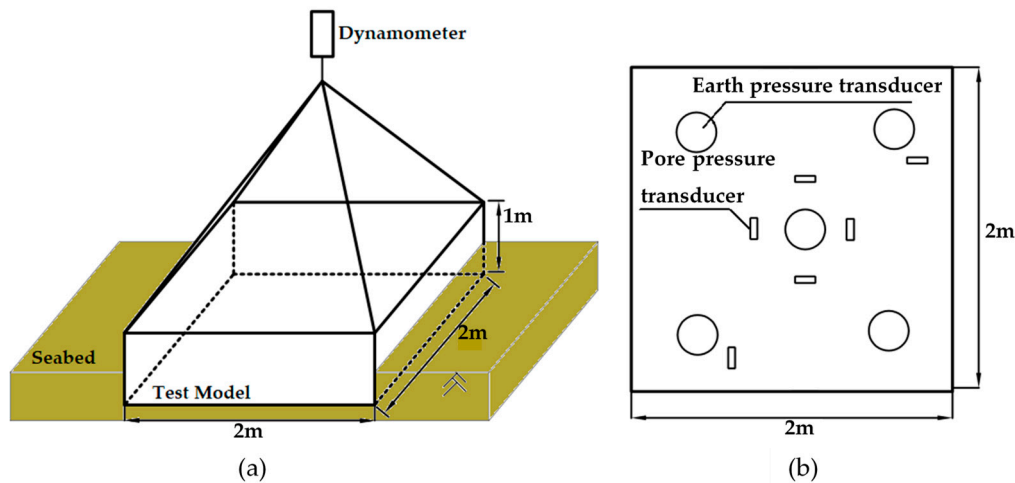


Figure 2. (a) Overall and (b) bottom schematic diagram of the bottom-supported model foundation.

2.2. Test Principles

The purpose of this test was to measure the buoyancy variation of the model box during the entire sitting time. The test model can calculate the buoyancy on the basis of the water pressure difference between top and bottom surface and the effective stress at the bottom of the model. Since the model box was a rectangular parallelepiped, the pressure on the side walls was offset reciprocally by the walls. Figure 3 shows the principle of this test. Because of the relatively large bottom area of the model box, only the lower part was embedded in the seabed. The top surface of the model box was subjected to water pressure. The bottom surface of the model box was subjected to water pressure and to the support force of the seabed. In the first method (Figure 3a), only the water pressure on the top and bottom surface was considered, and the buoyancy was equal to the water pressure difference between them. The buoyancy can be expressed as follow:

$$F = (u_1 - u_2) \times A \tag{1}$$

where F is the buoyancy of the model box, u_1 is the pore water pressure measured by the bottom pore pressure transducer, u_2 is the pore water pressure measured by the top pore pressure transducer, and A is the bottom area of the model.

In the second method (Figure 3b), the concept of effective stress was introduced. It is considered that the self-weight of the model is balanced by the buoyancy and the effective support force from the seabed. Hence, the buoyancy can be expressed as follow:

$$F = G - P \tag{2}$$

$$P = (w - u_1) \times A \tag{3}$$

where G is the self-weight of the model, P is the effective support force of seabed, and w is the total stress measured by the bottom earth pressure transducer.

In order to eliminate the influence of uneven pressure on the bottom surface, when calculating the buoyancy, the readings of transducers installed at the bottom were averaged.

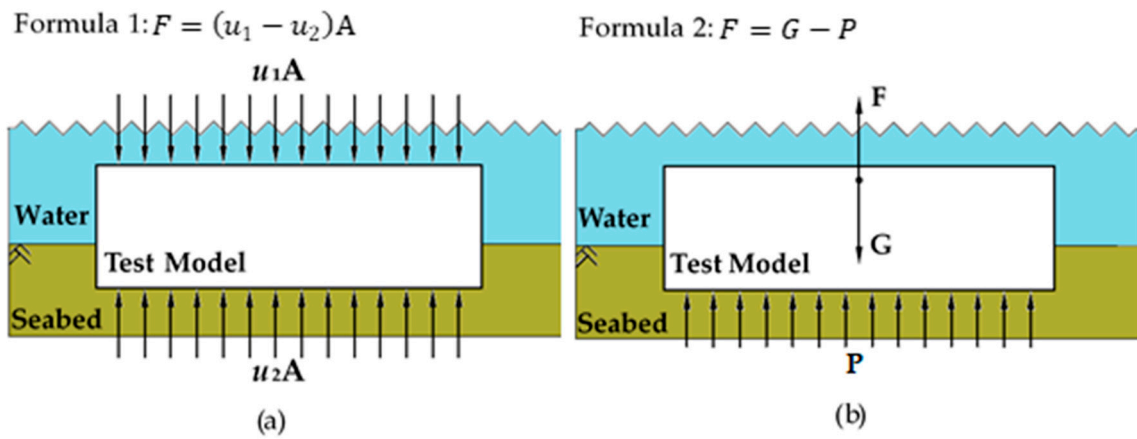


Figure 3. Schematic diagram of the test principle for (a) Formula 1 and (b) Formula 2.

2.3. Test Plan

The steps of the field tests were as follows: (1) number the transducers and calibrate their initial values before the start of the test; (2) connect all the parts correctly (crane, dynamometer, model box, transducers, data collector, and computer) and record the initial reading of the dynamometer (the weight of the model); (3) slowly sink the model into the sea until the dynamometer reading approaches zero; (4) continuously record the readings of the transducers until the preset sitting time; (5) pull up the steel box for the next test. Five tests with different sitting times were carried out to investigate the buoyancy acting on the model, as listed in Table 1. Figure 4 shows some photographs of the test.

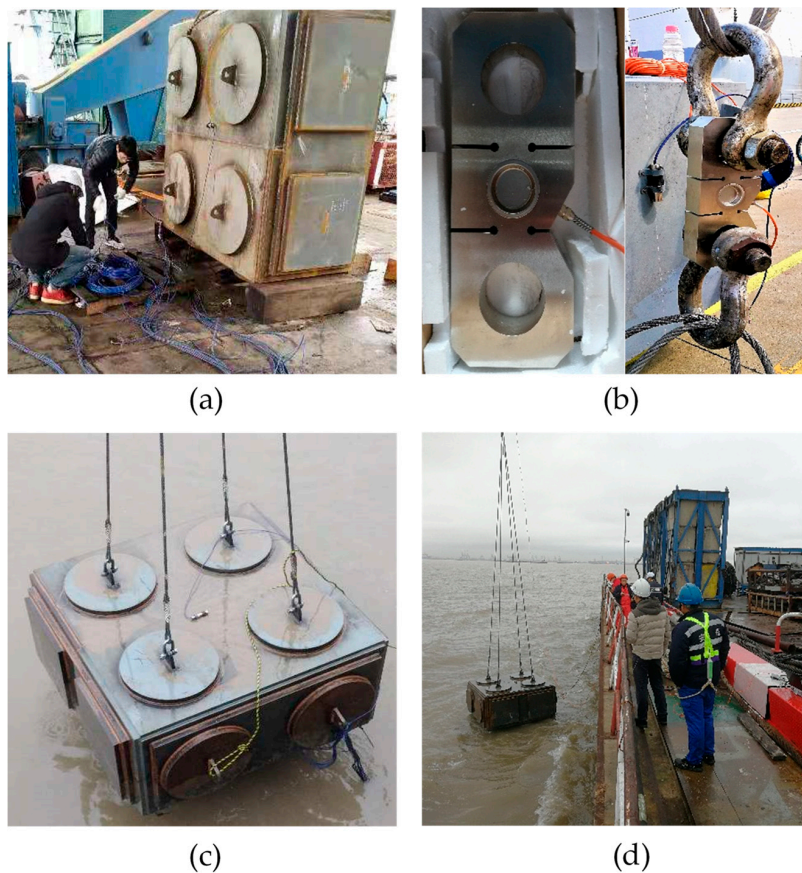


Figure 4. Photographs taken during the test: (a) numbering of the transducers and calibration of their initial values; (b) dynamometer used in the test; (c) lowering of the model to start the test; (d) test site.

Table 1. Test plan.

Test Case	a	b	c	d	e
Sitting time	3 h	6 h	22 h	2.5 days	5 days
Sampling frequency	every 1 min	every 1 min	every 10 min	every 10 min	every 10 min

2.4. Tests Results

Figure 5 shows the total stress and pore water pressure results during the sitting time of 3 h, 6 h, 22 h, 2.5 days, and 5 days. In Figure 5a,b, the sampling frequency was every 1 min, and in Figure 5c–e, the sampling frequency was every 10 min. The average total stress (\bar{w}) represents the mean of the readings of five bottom earth pressure transducers. The average bottom pore water pressure (\bar{u}_1) represents the mean of the readings of six bottom pore pressure transducers. The top pore water pressure (u_2) was obtained from the top pore pressure transducer. The test results in Figure 5 are fluctuating because of the influence of tides. The state of the tide at the beginning stage of each test can be obtained according to u_2 . At the beginning of Case a, the tide was rising, and at the beginning of Cases b, c, d, e, the tide was falling. The initial phase of the tide had an influence on the readings of the transducers (as shown by the difference between Case a and Case b) but had no effect on the variation of the buoyancy, since both methods of calculating buoyancy are based on subtraction. As the sitting time increased, the result of \bar{u}_1 showed a decreasing trend, which is shown in Figure 5e (the dotted red line is the trend line for \bar{u}_1). On the basis of the tests results, the buoyancy variation of the model was determined during a long sitting time. Therefore, further discussion on pore pressure difference, effective stress, and buoyancy is based on the sitting time of 5 days.

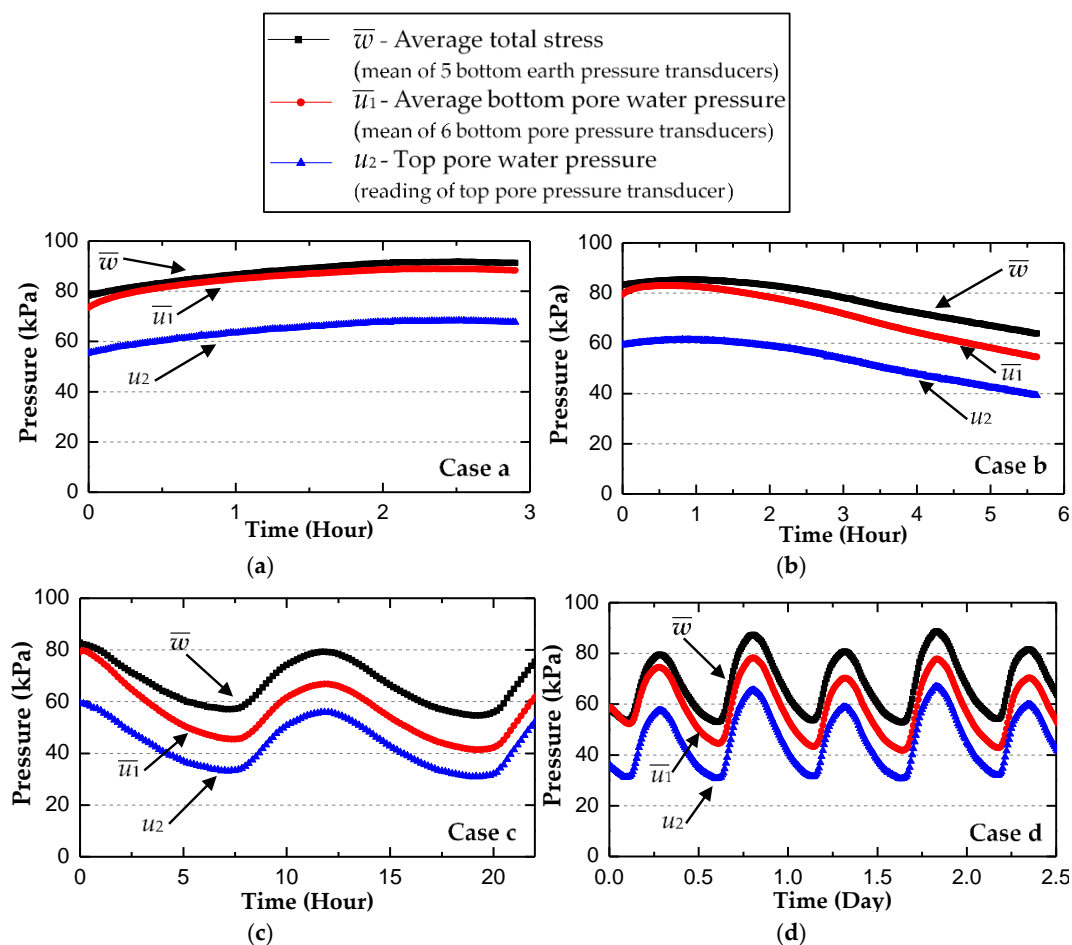


Figure 5. Cont.

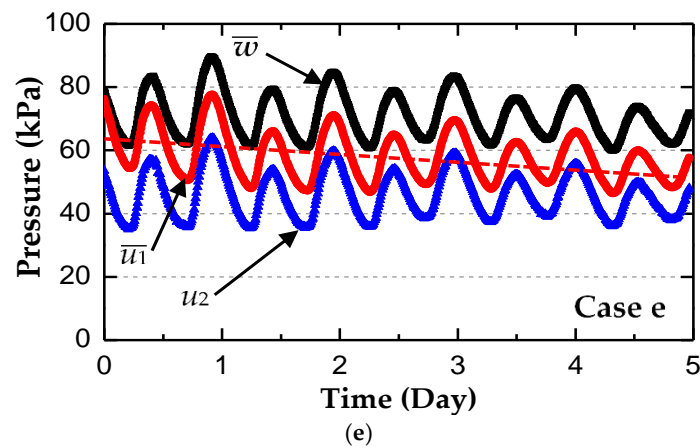


Figure 5. Field test results of total stress and pore water pressure during the sitting time of (a) 3 h, (b) 6 h, (c) 22 h, (d) 2.5 days, and (e) 5 days.

Figure 6 shows the variation of the pore pressure difference and effective stress during 5 days, calculated from the aforementioned field test results. The pore pressure difference is obtained by the difference between the average bottom pore water pressure and the top pore water pressure ($\bar{u}_1 - u_2$). When the model was completely submerged in the sea, the theoretical value of the pore pressure difference was 10 kPa, since the height was 1 m. The sitting process of the model is considered to be an undrained compression. The external load was almost completely borne by the pore water because of the low permeability of the seabed at the initial stage. Significant excess pore pressure was generated at the bottom of the model. As the sitting time increased, the excess pore pressure gradually dissipated and eventually stabilized at the theoretical value. When calculating the difference, it appeared that the influence of the tide on the pore pressure difference was almost eliminated, but a slight fluctuation was still visible. This phenomenon can be attributed to the phase lag of the pore pressure response caused by the low permeability of the seabed. When the water level changed due to the tide, the response of the top pore pressure transducer was instantaneous. However, the response of the bottom pore pressure transducer was very slow compared to that of the top one, since the lower half of the model was embedded in the lowly permeable seabed. The phase lag in the pore pressure response between the two places has also been reported in many studies [13,14]. The effective stress is the average total stress minus the average bottom pore water pressure ($\bar{w} - \bar{u}_1$). The variation trend of the effective stress was completely opposite to that of the pore pressure difference. At the initial stage of the sitting time, the effective stress of the soil was at a low level because of the significant excess pore pressure. With the dissipation of the excess pore pressure, the effective stress gradually accumulated and eventually stabilized at about 15 kPa

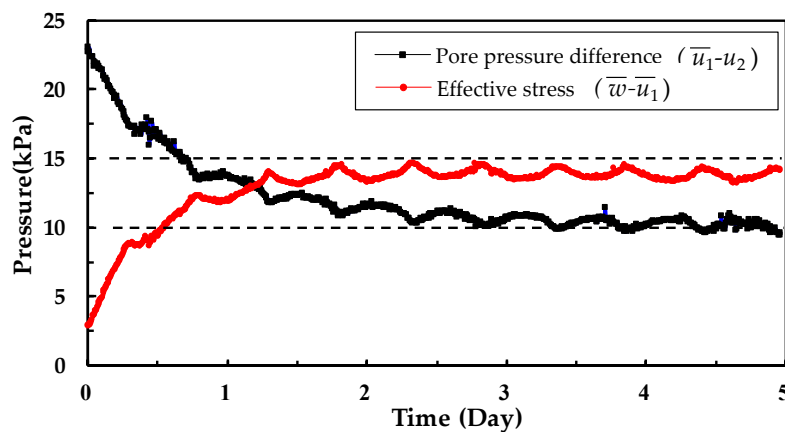


Figure 6. Variation of the pore pressure difference and effective stress during the sitting time of 5 days.

Figure 7 shows the variation of buoyancy during 5 days, which was based on the pore pressure difference and the effective stress. The trend of the buoyancy results obtained by the two methods was consistent. The results indicated that the model was subjected to buoyancy during the entire sitting time because of the connectivity of the pore water in the seabed to the outside seawater. At the beginning of the sitting time, the buoyancy could reach twice the theoretical value as a result of the significant excess pore pressure at the bottom of the model. With the dissipation of the excess pore pressure (increase of the effective stress), the buoyancy decreased and eventually stabilized near the theoretical value. The fluctuation of the buoyancy was consistent with that of the pore pressure difference and effective stress.

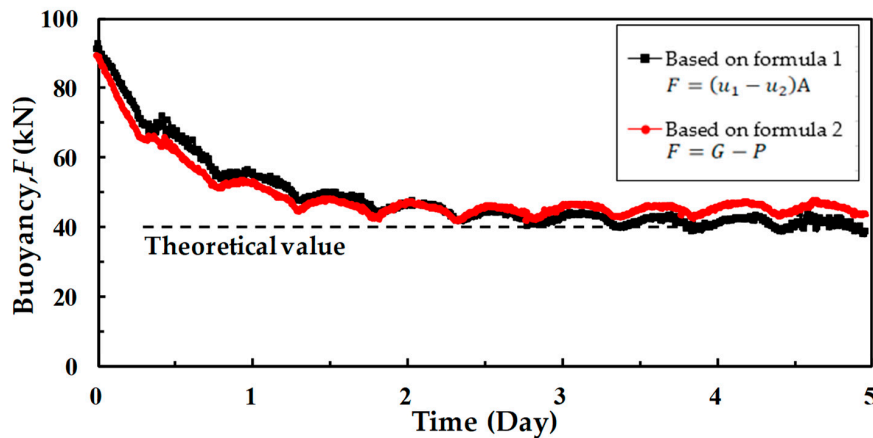


Figure 7. Variation of buoyancy (based on two calculation methods) during the sitting time of 5 days.

3. Numerical Simulation

In order to exclude the contingency of field results, since tests were conducted only in one place, the numerical coupled analysis was performed to verify the dissipation of the excess pore pressure at the bottom of the model foundation. Furthermore, the numerical result of buoyancy based on the pore pressure difference was also obtained, but the effect of tides was not taken into account. Some scholars have investigated the pore pressure response of seabed soil by fluid–solid coupling numerical analysis [15–18]. The dissipation process of the excess pore pressure in the field test was due to the consolidation of the soil after being subjected to external loads [19,20]. The analysis was performed with the software Abaqus.

3.1. Soil Property

The MCC model was used to simulate the behavior of the seabed soil, and the soil was considered homogeneous and normally consolidated. Such an approximation is appropriate for simulating the pore pressure dissipation. The parameters of the MCC model are summarized in Table 2. These parameters are empirical values based on existing Shanghai clay parameters [21–23].

Table 2. Parameters of the Modified Cam Clay (MCC) model.

Parameter	Symbol	Value
Slope of normally consolidated line in $e - \ln p'$ space	λ	0.2
Slope of swelling and recompression line in $e - \ln p'$ space	κ	0.04
Slope of critical state line in $p' - q$ space	M	1.2
Poisson's ratio	ν	0.3
Void ratio at $p' = 1$ kPa on critical line	e_{cs}	1.28
Permeability	k (m/s)	10^{-9}
Saturated bulk density of soil,	γ (kN/m ³)	18
Coefficient of earth pressure	K_0	0.6

According to the theory of the MCC model, the initial size of yield surface can be expressed as:

$$p'_0 = \frac{q^2}{M^2 p'} + p' \tag{4}$$

where M is the slope of the critical state line in $p' - q$ space, and p' and q are mean effective stress and deviatoric stress, respectively. The initial void ratio varies with depth, which is expressed by:

$$e_0 = e_1 - \lambda \ln p'_0 + \kappa \ln \frac{p'_0}{p'}, \tag{5}$$

where e_1 is the void ratio at $p' = 1$ kPa on the normally consolidated line, λ is the slope of the normally consolidated line in $e - \ln p'$ space, and κ is the slope of the swelling and recompression line in $e - \ln p'$ space.

$$e_1 = e_{cs} + (\lambda - \kappa) \ln(2) \tag{6}$$

3.2. Model and Mesh

A two-dimensional model was built to demonstrate the dissipation of the excess pore pressure. As shown in Figure 8, the model foundation was considered to be a rigid body with a width of 2 m. The soil was 20 m and 10 m long in the horizontal and vertical directions, respectively, to eliminate boundary interference. The CPE4P (four-node plane strain quadrilateral, bilinear displacement, bilinear pore pressure) elements were used in the model. Finer meshes were used on the upper part of the soil to improve the analysis accuracy. The structure and the soil were bound, since the contact between them was considered rough during the whole sitting process [24,25]. Of all the boundaries, only the upper surface of the soil was considered to be permeable. The sitting process was considered to be an undrained compression. Force-controlled analysis was used in the simulation, and the external load was the weight of the model box minus the theoretical buoyancy. The consolidation time was 5 days.

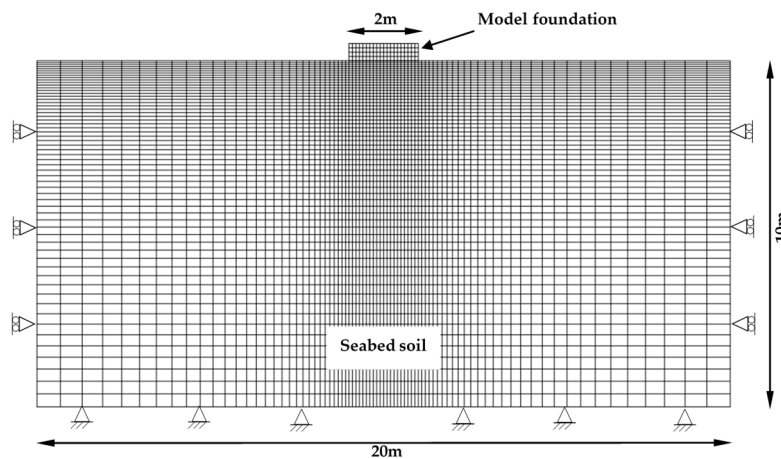


Figure 8. Model and mesh of the numerical analysis.

3.3. Comparison between Numerical Analysis and Field Test

The dissipation of the excess pore pressure at the bottom of the model foundation was obtained from the numerical analysis. Figure 9 presents the distribution of the excess pore pressure within the 4 m depth after different sitting times. At the initial stage of the sitting time, the excess pore pressure was significant and concentrated at the corner of the model foundation, as shown in Figure 9a. With the increase of the sitting time, the excess pore pressure of the seabed surface dissipated first, while the excess pore pressure in the deep was still significant, as shown in Figure 9d. The peak value of the excess pore pressure decreased as the sitting time increased. The simulation value of the pore pressure

difference was composed of the average excess pore pressure at the bottom of the model foundation and a fixed value of 10 kPa, which was determined by the height of the model foundation. The simulation result was a smooth curve, since the influence of tides was not considered in the numerical analysis. In Figure 10, two buoyancy curves based on the pore pressure difference are presented (one is the measured value and the other is the simulation value). The agreement between the simulated results and the measured results was acceptable. Therefore, the pore pressure obtained in the field test and the calculated buoyancy were considered reasonable. According to the results from the numerical analysis, the deep excess pore pressure had little effect on the buoyancy acting on the model foundation.

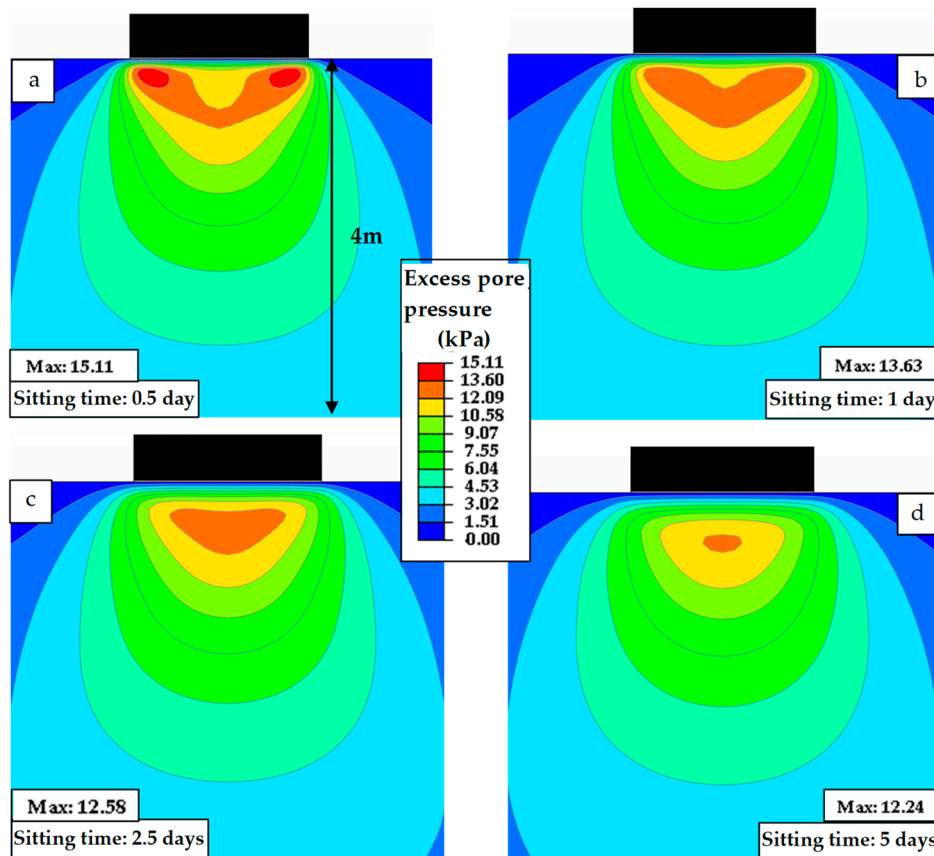


Figure 9. Distribution of the excess pore pressure after sitting for (a) 0.5 day, (b) 1 day, (c) 2.5 days, and (d) 5 days.

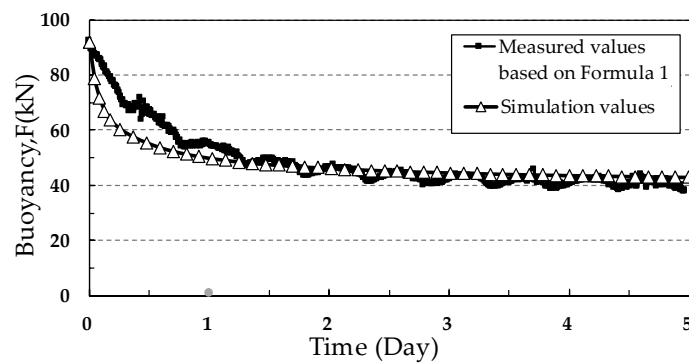


Figure 10. Comparison of buoyancy between numerical analysis and field test.

4. Conclusions

A model box comparable to the real field condition was designed to simulate the bottom-supported foundation, and transducers were installed on both top and bottom surfaces of the box. Field tests with different sitting times were carried out to investigate the buoyancy acting on the model box. Two different methods were used to calculate the buoyancy based on the test results. The main focus of this paper was on the dissipation of excess pore pressure at the bottom of the model and on the variation of buoyancy during the entire sitting time. Moreover, a numerical coupled analysis based on normal consolidation soil was carried out to verify the field tests results. The following conclusions can be drawn:

- (a) The model foundation was subjected to buoyancy during the entire sitting time because of the connectivity of the pore water in the seabed to the outside seawater.
- (b) At the initial stage of the sitting time, the buoyancy of the model could reach twice the theoretical value. As the sitting time increased, the buoyancy gradually decreased and eventually stabilized near the theoretical value. The fluctuation of buoyancy was due to the difference of the pore pressure response speed between the top and the bottom surfaces when the water level changed. The pore pressure response of the bottom surface had a phase lag relative to that of the upper surface, since the lower half of the model was buried in the lowly permeable seabed.
- (c) The soil–water coupled numerical analysis demonstrated that the buoyancy acting on the model was closely related to the pore water pressure at the bottom of the model. The buoyancy reached twice the theoretical value at the beginning as a consequence of the significant excess pore pressure at the bottom. With the dissipation of the excess pore pressure at the surface of the seabed, the buoyancy decreased. The deep excess pore pressure had little effect on the buoyancy acting on the model foundation.

During operation, a bottom-supported foundation is mainly subjected to two processes, that is, the sitting process and the uplifting process. The research of this paper mainly focused on the sitting process of the foundation. Further work will focus on the uplifting process of the foundation. During the uplifting process, the foundation is subject to resistance mainly caused by the negative pore pressure, which we call the bottom separation force. Both experimental and numerical studies will be conducted to explore (i) the formation mechanism of the bottom separation force, (ii) the factors affecting the bottom separation force, and (iii) the measures necessary to reduce the bottom separation force. This will provide a reference for practical engineering.

Author Contributions: Conceptualization, G.Y. and L.Z.; Data curation, S.P.; Formal analysis, T.F.; Methodology, G.Y.; Project administration, G.L. and H.S.; Writing—original draft, T.F.; Writing—review & editing, G.Y.

Funding: The authors are grateful for the financial support from the National Natural Science Foundation of China (Grant No. 41727802, 41630633) and the Science and Technology Commission of Shanghai Municipality (STCSM) (Grant No. 18DZ1100100).

Acknowledgments: The valuable discussions with Chencong Liao during the tests are appreciated.

Conflicts of Interest: The authors declare no conflict of interest.

References

1. Zhang, Q.; Ouyang, L.; Wang, Z.; Liu, H.; Zhang, Y. Buoyancy Reduction Coefficients for Underground Silos in Sand and Clay. *Indian Geotech. J.* **2018**, *49*, 1–8. [[CrossRef](#)]
2. Xiang, K.; Zhou, S.; Zhan, C. Model test study of buoyancy on shallow underground structure. *J. Tongji Univ. (Nat. Sci.)* **2010**, *38*, 346–357. [[CrossRef](#)]
3. Mohri, Y.; Fujita, N.; Kawabata, T. A Simulation on Uplift Resistance of Buried Pipe by DEM. In *Proceedings of the Pipelines 2001: Advances in Pipelines Engineering and Construction, San Diego, CA, USA, 15–18 July 2001*; ASCE: Reston, VA, USA, 2004.

4. Suenaga, S.; Mohri, Y.; Matsushima, K. Performance of Shallow Cover Method with Geogrid at Large Blasting Test. In *Proceedings of the Pipeline Engineering and Construction International Conference, Baltimore, Maryland, USA, 13–16 July 2003*; ASCE: Reston, VA, USA, 2003.
5. Chian, S.C.; Tokimatsu, K.; Madabhushi, S.P.G. Soil Liquefaction–Induced Uplift of Underground Structures: Physical and Numerical Modeling. *J. Geotech. Geoenviron. Eng.* **2014**, *140*, 1–18. [[CrossRef](#)]
6. Song, L.; Wang, Y.; Fu, L.; Mei, G.X. Test and analysis on buoyancy of underground structure in soft clay. *Rock Soil Mech.* **2018**, *39*, 753–758. [[CrossRef](#)]
7. Song, L.; Kang, X.; Mei, G. Buoyancy force on shallow foundations in clayey soil: An experimental investigation based on the “Half Interval Search”. *Ocean Eng.* **2017**, *129*, 637–641. [[CrossRef](#)]
8. Achari, G.; Joshi, R.C.; Bentley, L.R.; Chatterji, S. Prediction of the hydraulic conductivity of clays using the electric double layer theory. *Canada Geotech. J.* **1999**, *36*, 783–792. [[CrossRef](#)]
9. Singh, P.N.; Wallender, W.W. Effects of Adsorbed Water Layer in Predicting Saturated Hydraulic Conductivity for Clays with Kozeny–Carman Equation. *J. Geotech. Geoenv. Eng.* **2008**, *134*, 829–836. [[CrossRef](#)]
10. Zhang, J.; Cao, J.; Mu, L.; Wang, L.; Li, J. Buoyancy Force Acting on Underground Structures considering Seepage of Confined Water. *Complexity* **2019**, *2019*, 7672930. [[CrossRef](#)]
11. Gu, X.; Zhou, T.; Cheng, S. The Soft Soil Foundation Consolidation Numerical Simulation Based on the Model of Modified Cam-Clay. *Appl. Mech. Mater.* **2014**, *580*, 3223–3226. [[CrossRef](#)]
12. Lim, Y.X.; Tan, S.A.; Phoon, K.-K. Interpretation of horizontal permeability from piezocone dissipation tests in soft clays. *Comput. Geotech.* **2019**, *107*, 189–200. [[CrossRef](#)]
13. Zen, K.; Yamazaki, H. Mechanism of wave-induced liquefaction and densification in seabed. *Soils Found.* **1990**, *30*, 90–104. [[CrossRef](#)]
14. Yamamoto, T.; Koning, H.L.; Sellmeijer, H.; Hijum, E.V. On the response of a poro-elastic bed to water waves. *J. Fluid Mech.* **1978**, *87*, 193–206. [[CrossRef](#)]
15. Liao, C.; Chen, J.; Zhang, Y. Accumulation of pore water pressure in a homogeneous sandy seabed around a rocking mono-pile subjected to wave loads. *Ocean Eng.* **2019**, *173*, 810–822. [[CrossRef](#)]
16. Liao, C.; Tong, D.; Chen, L. Pore Pressure Distribution and Momentary Liquefaction in Vicinity of Impermeable Slope-Type Breakwater Head. *Appl. Ocean. Res.* **2018**, *78*, 290–306. [[CrossRef](#)]
17. Jeng, D.-S.; Ye, J.H. Three-dimensional consolidation of a porous unsaturated seabed under rubble mound breakwater. *Ocean Eng.* **2012**, *53*, 48–59. [[CrossRef](#)]
18. Ye, G.-L.; Leng, J.; Jeng, D.-S. Numerical testing on wave-induced seabed liquefaction with a poro-elastoplastic model. *Soil Dyn. Earthq. Eng.* **2018**, *105*, 150–159. [[CrossRef](#)]
19. Zheng, J.-J.; Lu, Y.-E.; Yin, J.-H.; Guo, J. Radial consolidation with variable compressibility and permeability following pile installation. *Comput. Geotech.* **2010**, *37*, 408–412. [[CrossRef](#)]
20. Gaudin, C.; Li, X.; Tian, Y.; Cassidy, M.J. About the uplift resistance of subsea structure. In *Proceedings of the 19th International Conference on Soil Mechanics and Geotechnical Engineering, Seoul, Korea, 17–21 September 2017*; ISSMGE: London, UK, 2017.
21. Ye, G.; Ye, B. Investigation of the overconsolidation and structural behavior of Shanghai clays by element testing and constitutive modeling. *Undergr. Space* **2016**, *1*, 62–77. [[CrossRef](#)]
22. Zhang, S.; Ye, G.; Wang, J. Elastoplastic Model for Overconsolidated Clays with Focus on Volume Change under General Loading Conditions. *Int. J. Geomech.* **2018**, *18*, 1–14. [[CrossRef](#)]
23. Zhang, S.; Ye, G.; Liao, C.; Wang, J. Elasto-plastic model of structured marine clay under general loading conditions. *Appl. Ocean. Res.* **2018**, *76*, 211–220. [[CrossRef](#)]
24. Li, X.; Tian, Y.; Gaudin, C.; Cassidy, M.J. Comparative study of the compression and uplift of shallow foundations. *Comput. Geotech.* **2015**, *69*, 38–45. [[CrossRef](#)]
25. Yadav, S.K.; Ye, G.-L.; Xiong, Y.-L.; Khalid, U. Unified numerical study of shallow foundation on structured soft clay under unconsolidated and consolidated-undrained loadings. *Mar. Georesour. Geotech.* **2019**, 1–17. [[CrossRef](#)]

